

# A correlation for turbulent combustion speed accounting for instabilities and expansion speed in a hydrogen-natural gas spark ignition engine

Blanca Giménez<sup>a,\*</sup>, Andrés Melgar<sup>a</sup>, Alfonso Horrillo<sup>b</sup>, Francisco V. Tinaut<sup>a</sup>

<sup>a</sup> Department of Energy and Fluid Mechanics Engineering, University of Valladolid, Paseo del Cauce 59, E-47011 Valladolid, Spain

<sup>b</sup> CIDAUT Foundation, Plaza Vicente Aleixandre Campos 2, Parque Tecnológico, E-47151 Boecillo-Valladolid, Spain

## ARTICLE INFO

### Article history:

Received 26 February 2020

Revised 20 September 2020

Accepted 21 September 2020

Available online 13 October 2020

### Keywords:

Quasi-dimensional combustion diagnosis

Turbulent combustion speed

Natural gas – hydrogen mixtures

Premixed combustion

Internal combustion engine

Instabilities

Expansion speed

## ABSTRACT

An analysis of the turbulent premixed combustion speed in an internal combustion engine using natural gas, hydrogen and intermediate mixtures as fuels is carried out, with different air-fuel ratios and engine speeds. The combustion speed has been calculated by means of a two-zone diagnosis thermodynamic model combined with a geometric model using a spherical flame front hypothesis. 48 operating conditions have been analyzed. At each test point, the pressure record of 200 cycles has been processed to calculate the cycle averaged turbulent combustion speed for each flame front radius. An expression of turbulent combustion speed has been established as a function of two parameters: the ratio between turbulence intensity and laminar combustion speed and the second parameter, the ratio between the integral spatial scale and the thickness of the laminar flame front increased by instabilities. The conclusion of this initial study is that the position of the flame front has a great influence on the expression to calculate the combustion speed. A unified correlation for all positions of the flame front has been obtained by adding one correction term based on the expansion speed as a turbulence source. This unified correlation is thus valid for all experimental conditions of fuel types, air-fuel ratios, engine speeds, and flame front positions. The correlation can be used in quasi-dimensional predictive models to determine the heat released in an ICE.

© 2020 The Authors. Published by Elsevier Inc. on behalf of The Combustion Institute.  
This is an open access article under the CC BY license (<http://creativecommons.org/licenses/by/4.0/>)

## 1. Introduction

In most industrial applications, the combustion processes appear in a turbulent regime, so the turbulence effect increases combustion speed and then the thermal power per unit volume increases. The kinetic energy due to the fluid movement is degraded by eddies generation that are dissipated by friction, but at the same time this causes an important increase of the diffusion effects. The combustion speed resulting from the flow turbulence is several times higher than the one that would exist in a non-turbulent process (laminar). An analytical expression of the combustion speed, depending on pressure, temperature, reactants and turbulence levels, helps to design combustion devices.

The influence of the turbulence on the combustion process can be very different depending on the turbulence intensity and length levels relative to the reaction variables (laminar speed and flame

width). An attempt to classify the different combustion regimes is presented in the Borghi diagram [1].

Many experimental and theoretical works have tried to find the dependence of the turbulent combustion speed and the involved parameters [2,3] in free field flames. There are reviews that classify the large number of works carried out in this field and their application in predictive models [4].

The premixed combustion process development caused by a flame front advancing in a quiescent fluid is governed by both mass and thermal diffusivities that cause the reaction to progress towards the fresh mixture zone. The reaction rates governed by chemical kinetics, which depend mainly on temperature and reactant concentration, also influence the process. The laminar combustion speed depends on all these phenomena, and can be calculated by using one-dimensional models that consider transport phenomena and reaction kinetics [5,6]. In many conditions of pressure, temperature and air-fuel ratio the laminar combustion speed cannot be determined experimentally since the combustion process distorts the fluid movement generating instabilities.

\* Corresponding author.

E-mail addresses: [blagim@eii.uva.es](mailto:blagim@eii.uva.es) (B. Giménez), [andmel@eii.uva.es](mailto:andmel@eii.uva.es) (A. Melgar), [alfhor@cidaut.es](mailto:alfhor@cidaut.es) (A. Horrillo), [tinaut@eii.uva.es](mailto:tinaut@eii.uva.es) (F.V. Tinaut).

**NOMENCLATURE**

<i>A</i>	area (m <sup>2</sup> )
<i>ICE</i>	Internal Combustion Engine
<i>c</i>	specific heat (J/kgK)
<i>CFD</i>	Computational Fluid Dynamics
<i>D</i>	diameter (m)
<i>D</i>	mass diffusivity (m <sup>2</sup> /s)
<i>Da</i>	Damköhler number $(L_I/\delta_L)/(u'/S_I)$
<i>DL</i>	Darrieus Landau
<i>E</i>	overall activation energy (J/kg)
<i>ECU</i>	Engine Control Unit
<i>h</i>	specific enthalpy (J/kg). Film coefficient (W/m <sup>2</sup> K)
<i>H<sub>p</sub></i>	heating value per kg of reactive (J/kg)
<i>K<sub>w</sub></i>	multiplier of Woschni film coefficient
<i>K<sub>a</sub></i>	Karlovitz number $(u'/S_I)/(L_K/\delta_I)$
<i>L</i>	turbulent length scale (m)
<i>ℓ</i>	Markstain length (m)
<i>Le</i>	Lewis number $\alpha/D$
<i>LES</i>	Large Eddy Simulation
<i>m</i>	mass (kg)
<i>MFB</i>	mass fraction burned
<i>p</i>	pressure (Pa)
<i>P</i>	perimeter (m)
<i>Pr</i>	Prandtl number $\nu/\alpha$
<i>q</i>	incoming heat per mass unit (J/kg)
<i>Q</i>	incoming heat to the system (J)
<i>r</i>	radial coordinate from the piston axis (m)
<i>rms</i>	root mean square
<i>R</i>	radius (m)
<i>R</i>	gas ideal constant (J/kgK)
<i>RANS</i>	Reynolds Averaged Navier Stokes
<i>Re</i>	Reynolds number $SL/\nu$
<i>S</i>	combustion speed, speed (m/s)
<i>t</i>	time (s)
<i>T</i>	temperature (K)
<i>TDC</i>	top dead center
<i>u</i>	specific internal energy (J/kg)
<i>u'</i>	intensity of isotropic turbulence (m/s)
<i>v</i>	specific volume (m <sup>3</sup> /kg)
<i>V</i>	volume (m <sup>3</sup> )
<i>y</i>	axial coordinate from the piston top (m)
<i>Y</i>	mass fraction (dimensionless)
<i>Z</i>	number of species

*Greek letters*

$\alpha$	crankshaft angle (rd). Thermal diffusivity (m <sup>2</sup> /s) $\kappa/\rho c_p$
$\beta$	Zel'dovich number $(E(T_b - T_u)/R T_b^2)$
$\delta$	thickness of flame front (m)
$\phi$	fuel-air equivalence ratio
$\gamma$	specific heats ratio (dimensionless)
$\kappa$	thermal conductivity (W/mK)
$\lambda$	wavelength (m)
$\mu$	dynamic viscosity (N s/m <sup>2</sup> )
$\nu$	kinematic viscosity (m <sup>2</sup> /s)
$\theta$	angle from the piston axis (rd)
$\rho$	density (kg/m <sup>3</sup> )
$\sigma$	density ratio $\rho_u/\rho_b$
$\omega$	amplitude growth rate (1/s)

*Subscripts*

<i>ac</i>	admission valve close
<i>B</i>	bowl

<i>b</i>	burned
<i>bb</i>	blow-by
<i>cf</i>	confined field
<i>D</i>	displaced
<i>DL</i>	Darrieus Landau
<i>e</i>	expansion
<i>eff</i>	effective
<i>f</i>	flame front
<i>ff</i>	free field
<i>fin</i>	final
<i>ini</i>	initial
<i>I</i>	integral
<i>K</i>	Kolmogorov
<i>l</i>	laminar
<i>m</i>	motored engine
<i>p</i>	piston
<i>t</i>	turbulent
<i>t<sub>∞</sub></i>	turbulent in free field
<i>u</i>	unburned
<i>v</i>	constant volume

*Superscripts*

*	correction considering species dissociation
#	simplified expression

Under conditions of laminar combustion, when the flame front advances into the reactants, a density decrease occurs which induces a movement in the reactants zone, or of the products or on both sides of the flame front, depending on the flow confinement conditions. If this movement is not balanced in all points, the flame front can be deformed increasing the reaction surface. Consequently, the amount of reactants consumed per unit of time increases with respect to the laminar process. Detailed reviews of the state of the art of the analysis of the combustion instabilities can be found in [7–9], where it is concluded that a disturbance on the flame front of a wavelength, the combustion process can be unstable or stable depending on the properties of the reactive mixture. It is also concluded that under conditions of low levels of turbulence these instabilities can influence the forward speed of the flame front on the reactants.

The premixed combustion process in the internal combustion engine (ICE) has specific characteristics. First, the flow is non-stationary, but markedly cyclic because of the reciprocating piston motion. Second, the flow velocities inside the combustion chamber are proportional to the average piston speed [10–12]. These velocities are generated mainly by intake and compression processes. Correspondingly, the turbulence intensity is proportional to the engine speed [12–15]. Third, the combustion chamber walls confine the flow and the distance between them determines the integral length scale [10,14,16]. And finally, the combustion modifies the flow and consequently the process itself affects the turbulence levels [13,17].

In internal combustion engines, the flame is far from being in free field because it is confined and strongly affected by geometry. The turbulent premixed combustion regime is developed in moderate turbulence levels and eddies sizes much greater than the laminar flame front thickness [18]. On the other hand, it is a highly transient process since from the beginning, with approximately a 1 mm<sup>3</sup> volume, until the end, when the flame front reaches the walls of the cylinder and extinguishes, only a few milliseconds take place. Additionally, the pressure and temperature conditions are very high and transient. Under pressure and temperature conditions in an ICE, it is possible that the turbulent combustion speed  $S_t$  is affected by the both effects turbulence and instabilities [19].

The two most common methodologies used for modeling the premixed combustion process in internal combustion engines are the use of thermodynamic models and CFD models. The main advantage of the thermodynamic models is the very low calculation time.

Thermodynamic models are based on considering several zones (usually two zones) inside the combustion chamber where the flow properties are assumed to be uniform in each zone. The combination with a geometrical submodel that defines the flame front area as function of burned mass volume, provide a quasidimensional character. The burned mass rate at a certain moment is given by:

$$\frac{dm_b}{dt} = A_f \rho_u S_t$$

where  $A_f$  is the area of a smooth flame front unaffected by the turbulence. The turbulent combustion speed,  $S_t$ , has to be estimated from the process variables in terms of reactivity and diffusivity. The most influential parameters are the laminar combustion speed, the turbulence intensity and the integral length scale. There are several theories to calculate the turbulent combustion speed from these parameters, like the fractal theory [20], the turbulent entrainment models [21] and the correlations based on both reaction and eddies turnaround times. The latter are based on exponential expressions depending on turbulence characteristic dimensionless numbers [3], where the rates of turbulent to laminar combustion speeds is commonly used:

$$\frac{S_t}{S_l} = f \left( Re, Pr, Da, Ka, \frac{u'}{S_l}, \frac{L_l}{\delta_l} \right)$$

An example of thermodynamic models using this kind of expression for  $S_t/S_l$  can be found in [14], where the combustion duration is calculated in the ECU (Engine Control Unit) for all the operating conditions of an ignition engine with variable valve actuation system and charge motion control valves.

All these latter models utilize the mean turbulence intensity on the combustion chamber, usually calculated with models based on the differential equations of turbulence generation and dissipation during the intake process and the subsequent closed valves cycle [22].

In order to take into account the boundary conditions in an ICE, such as the proximity to the wall and the turbulent effects generated by the combustion itself, the models need adjustment constants depending on the combustion stages: initial, characterized by the turbulent combustion speed growth; intermediate, in which it remains more or less constant; and final, in which the speed decreases [11,13,23,24].

In [4,25] another modeling proposal is made. In this case, CFD based on RANS model is used. In this kind of models, the combustion chamber volume is discretized in cells and the conservation differential equations of Thermodynamics and fluid movement variables are integrated in each cell. In [26,27], additionally a conservative combustion progress variable is considered. The source and diffusive terms of the conservative equation for this variable depend on the turbulent combustion speed, which is a function of dimensionless numbers. The expression does not take into account the edge effects, since this kind of models are assumed to be able to predict the effects caused by the boundary conditions. An important handicap of this type of modeling with respect to quasidimensional models is a calculation time several orders of magnitude higher.

This is even more extreme for Large Eddy Simulation (LES) approaches where the dynamics of the larger eddies is computed and resolved in space and time [28].

Using a quasidimensional thermodynamic model in conjunction with the spark-centered spherical flame front hypothesis, the tur-

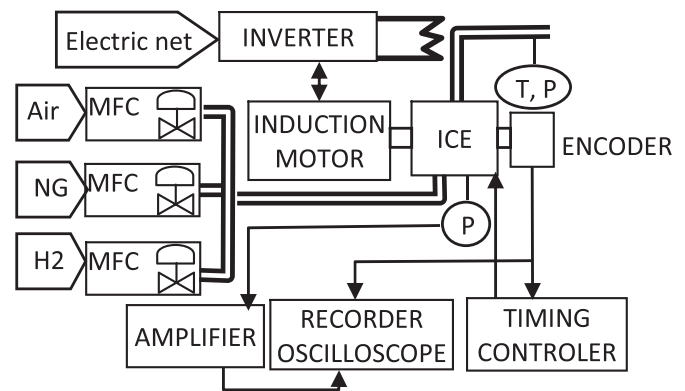


Fig. 1. Experimental facility.

bulent combustion rate can be estimated for each instant [29,30]. In this work, using the methodology described in [29] to process the chamber pressure data from an internal combustion engine, the turbulent combustion speed is calculated. This methodology is based on a quasidimensional thermodynamic model. An expression of the premixed turbulent combustion speed has been correlated as a function of the relevant variables. The expression is a function of commonly used dimensionless numbers, depending on laminar combustion speed and turbulence properties. The thickness of the laminar flame front has been modified taking into account the instabilities amplitude generated during a characteristic time related with the turbulence integral length scale and the laminar combustion speed. In addition, a new dimensionless number has been introduced in the  $S_t/S_l$  expression, depending on the boundary conditions existing in the combustion chamber through the expansion speed. The final objective is to use this expression in quasidimensional predictive models for calculate the heat release rate in the combustion process.

In order to modify the conditions in the combustion chamber, 48 engine tests with natural gas, hydrogen and mixtures of both were carried out, with different fuel-air ratios and engine speeds. In the experiments, the range of pressures during the combustion is between 1 and 3 MPa, while the temperature of the unburned mass is between 750 and 1000 K. Density ratios ( $\sigma = \rho_u/\rho_b$ ) are between 1.9 and 3.15.

The homogeneous combustion process in ICE is highly variable cycle by cycle and dependent on the position of the flame front within the combustion chamber. Therefore, the phenomenon can be expected to be more repetitive for the same position of the flame front as for the same angular position. For that, the cycle averaged turbulent combustion speeds have been calculated for the each averaged-flame front radius. The resulting combustion speed vs radius for all experimental tests have been compared at four representative flame front radius, in order to distinguish different combustion stages. Finally, the results of all test for the four flame front position have been correlated in a unified expression.

## 2. Experimental test and data preprocessing

Figure 1 shows the schematics of the experimental facility used in this work. The tests were carried out on a naturally aspirated internal combustion engine MINSEL 380, 380 cc single-cylinder, with an 80 mm piston diameter and a 75 mm stroke. The exhaust valve closes at the same angle that the intake valve begins to open, so there is not valve overlap. The engine is coupled to a 5.5 kW LEROY SOMER PLS 180 induction motor, controlled with a FUJI FRENIC-MEGA 7.5 kW frequency inverter. The electrical energy produced when the induction motor brakes the engine is dissipated on resistors.

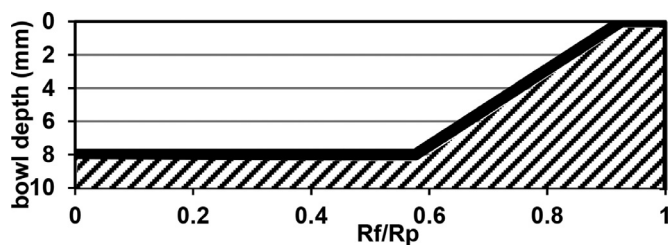


Fig. 2. Half piston geometry.

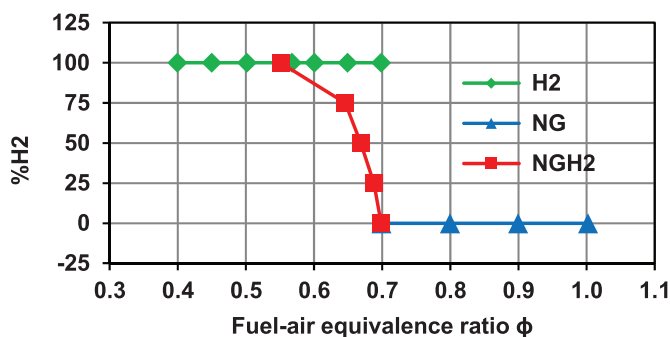


Fig. 3. Test plan for each engine speed.

The engine, originally a compression ignition engine, was transformed into a spark ignition one. A microprocessor controls the spark timing using the angular encoder signal. It was necessary to machine the piston axisymmetrically to reduce the compression ratio to 11.15. The half piston geometry is shown in Fig. 2.

BROOKS mass flow controllers (MFC in Fig. 1), specifically the 5853S model for air and the 5851S model for natural gas and hydrogen, are used. An AVL GU21D sensor is used for measuring the chamber pressure. An AVL 360C/600 angular encoder with 0.6 degrees resolution synchronizes the pressure signal and a KISTLER 5018A charge amplifier conditions it. Chamber pressure data synchronized with the encoder signal are recorded in a 16 bit YOKOGAWA DL750 oscilloscope. A low sampling frequency system measures average temperatures and other pressures.

An IDROENERGY 3.7 electrolyzer produces hydrogen at 1.5 bar and the natural gas is taken from the network at a pressure of 40 mbar above atmospheric pressure. Due to the pressure losses in the natural gas mass controller, the intake absolute pressure is limited to a maximum value of 0.8 bar. The air comes from a compressed air line.

Tests have been made recording pressure data in the combustion chamber during 200 consecutive cycles. The used fuels have been of three types.: Natural gas (NG) with several fuel-air equivalence ratios (1.0, 0.9, 0.8 and 0.7); Hydrogen (H<sub>2</sub>) with several fuel-air equivalence ratios (0.7, 0.65, 0.6, 0.55, 0.5, 0.45, 0.4); Mixtures of natural gas and hydrogen (NGH<sub>2</sub>) with different percentages of H<sub>2</sub> (0%, 25%, 50%, 75% and 100%) and fuel-air equivalence ratios (0.697, 0.686, 0.666, 0.633 and 0.536 respectively) adjusted to maintain the adiabatic flame temperature constant. For 100% natural gas and hydrogen tests, the lowest fuel-air equivalence ratio has been chosen which guarantee a stable engine behavior. The tested points are shown in Fig. 3.

Three engine speeds were tested: 1000, 1750 and 2500 rpm for each point, so that 48 tests were carried out.

The ignition angle is adjusted so that the maximum pressure is reached at 10° ATDC. The intake mass flow in each test is fixed to ensure that the number of admitted moles per cycle is the same for all tests. In this way, the pressure at the beginning of the compression is the same in all cases if the temperature is the same.

Then, the flow velocities through the intake valve are similar for all the tests with the same engine speed, and consequently the turbulence levels are similar for these tests as well.

Before applying the thermodynamic model presented in Section 3 to the pressure records, it is necessary to fix the exact value of four variables that have a great influence on the results. These variables are: the compression ratio, determined by the final piston geometry; the angular position of the pressure registers with respect to the TDC depending on the position of the encoder with respect to the crankshaft; the pressure offset, different in each cycle due to the use of a piezoelectric sensor; and the heat transfer coefficient to the walls of the combustion chamber. Although the latter is estimated with a correlation, a constant prefactor is needed in order to adapt the correlation to the engine tested.

Errors in determining the value of any of these variable can produce similar effects on the results of the obtained heat release. A first criterion used in this work is to select these four parameters in such a way that minimize the sum of the absolute values of the calculated heat released in each integration interval during the compression process (prior to combustion start). A second criterion also used is that the total heat released must be below the maximum possible.

To determine the optimal set of these values, global stochastic optimization methods have a greater probability of finding the global optimum in the entire range of variables than deterministic local optimization methods.

In this work, this optimization is done with a genetic algorithms approach. For each engine cycle of each test point, the thermodynamic model was applied 100 times to the pressure data using different combinations of these four parameters covering the entire range of variation of each one. These cases were evaluated using the objective function and those 10 with the best result were recombined to generate another set of 100 combinations of the parameters, this process took place over 25 generations. The results of all the cycles and all tests were analyzed and the optimal values of the compression ratio (11.15) and the angular reference were determined. The process was repeated varying only the heat transfer coefficient and the pressure offset. From the results of all cycles and all test points, the optimal value of the heat transfer coefficient was fixed to a common value of 0.8 for all test points. Finally, the pressure offset is determined, this variable is unique for each cycle. More information on this methodology, including the recombination method, can be found in [31].

Before processing the experimental data with the thermodynamic model, the pressure records are filtered in order to eliminate the experimental signal noise and improve the calculation of pressure derivatives. The filtering technique consists of calculating the value of pressure and its derivative using a fourth order polynomial. The polynomial coefficients are calculated by making a least squares fit using ten data prior to and another ten later than each calculation point. The *rms* value of the difference between experimental and filtered pressure is 1 kPa.

### 3. Combustion variables determination from experimental data

The tests pressure registers are processed to calculate the turbulent combustion speed  $S_f$  together with other variables that characterize the combustion process.

The used thermodynamic model allows calculating the burned mass rate,  $dm_b/dt$ , and the burned mass volume,  $V_b$ . This volume is an input of a geometric model that allows determining both the position radius  $R_f$ , and the area  $A_f$  of the spherical flame front. The hypothesis of spherical flame front implies that the turbulent combustion speed  $S_f$  and the flame front speed,  $dR_f/dt$ , are the same at all the points of the surface  $A_f$ .

With  $A_f$  and  $dm_b/dt$ , the turbulent combustion speed at each time can be calculated as:

$$S_t = \frac{\frac{dm_b}{dt}}{A_f \rho_u} \quad (1)$$

Also it is possible to calculate other variables such as the flame front speed,  $dR_f/dt$ , and the expansion speed,  $S_e$ . The latter corresponds to the velocity, in the perpendicular direction to the flame front, of the unburnt products located at the position of the flame front, called mean gas speed by Heywood [32].

The turbulence intensity,  $u'$ , in an ICE combustion chamber is difficult to measure specially in combustion condition [10–13,33,34]. In this work  $u'$  has been calculated by modeling the engine with the AVL BOOST code in motored engine conditions (more details in paragraph 3.4).

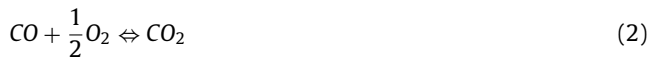
The laminar combustion speed, the diffusion properties and instabilities growth rate have been calculated from the thermodynamic conditions depending on the crank angle resolved conditions.

### 3.1. Thermodynamic model

The thermodynamic model distinguishes two differentiated zones, one zone corresponding the unburned mass  $m_u$ , and another zone corresponding to the burned mass  $m_b$ . The model is only used in the closed valves interval data.

The hypotheses used to propose the diagnostic model are the following, with their validity discussed in [35]:

- Uniform pressure in all the combustion chamber,  $p$ .
- A mean value of temperature in each zone,  $T_u$  and  $T_b$ .
- Ideal gas behavior depending on the composition of each zone is assumed, so the equation  $p\nu = RT$  is applied in each zone.
- The unburned mass zone composition does not vary with temperature, however, in the burned mass zone, the composition change is considered because of the displacement of the  $\text{CO}_2$  dissociation reaction:



It is considered that the reaction is in equilibrium since the temperature of the burned mass is high. The appearance of CO in the burned mass zone causes a decrease in the heat released by unit of burnt mass.

- No heat transfer is considered between the two zones, but there is heat transfer between the walls and each zones,  $q_u$  and  $q_b$ .
- There is a blow-by flow leakage,  $\dot{m}_{bb}$ , but only the unburned mass is lost from the combustion chamber through the piston contour.

Applying both the energy conservation and state equations in each zone, and the mass and volume conservation equations in all the volume, the following three differential equations are obtained, see [36]:

$$\frac{dm_b}{dt} = \frac{\frac{dp}{dt} \left( m_u \nu_u \frac{\gamma_b^*}{\gamma_u} + m_b \left( \nu_b + (\gamma_b^* - 1) \frac{\partial u_b}{\partial p} \right) \right) - \left( \frac{\gamma_u - 1}{\gamma_u} \gamma_b^* \dot{Q}_u + (\gamma_b^* - 1) \dot{Q}_b \right) + p \gamma_b^* \left( \frac{dV(\alpha)}{dt} + \nu_u \dot{m}_{bb} \right)}{\gamma_b^* (u_u - u_b) + (h_u - h_b)} \quad (3)$$

$$\frac{dm_u}{dt} = -\frac{dm_b}{dt} - \dot{m}_{bb} \quad (4)$$

$$\frac{du_u}{dt} = \left( \frac{dp}{dt} \nu_u + \dot{q}_u \right) \frac{1}{\gamma_u} \quad (5)$$

$$\frac{du_b}{dt} = \begin{cases} \left( \frac{dp}{dt} \left( \nu_u + (\gamma_b^* - 1) \frac{\partial u_b}{\partial p} \right) + \dot{q}_u \right) \frac{1}{\gamma_b^*} m_b \cong 0 \\ \frac{dm_b}{dt} \frac{(u_u - u_b)}{m_b} - \frac{dp}{dt} \frac{\nu_u m_u}{\gamma_u m_b} + \frac{1}{m_b} \left( (\gamma_u - 1) \dot{Q}_u + \dot{Q}_b \right) \\ - \frac{p}{m_b} \left( \frac{dV(\alpha)}{dt} + \nu_u \dot{m}_{bb} \right) m_b > 0 \end{cases} \quad (6)$$

$$c_{vb}^* = c_{vb} + \sum_{i=1}^{i=Z_b} \frac{\partial Y_{bi}}{\partial T} u_i(T_b) \quad \gamma_b^* = \frac{c_{vb}^* + R_b}{c_{vb}^*} \frac{\partial u_b}{\partial p} = \sum_{i=1}^{i=Z_b} \frac{\partial Y_{bi}}{\partial p} u_i(T_b)$$

The terms  $\gamma_b^*$  and  $\partial u_b/\partial p$  allow to take into account the composition variation in the burned mass zone for the  $\text{CO}_2$  dissociation due to the high temperatures. The values of  $\partial Y_{bi}/\partial T$  and  $\partial Y_{bi}/\partial p$  are determined by calculating the value of  $Y_{bi}$  taking into account the dissociation of  $\text{CO}_2$  at three points: at the calculation point, at another, where the temperature is increased 1 K and another in which the pressure is increased 1000 Pa. The blowby flow is determined by assuming isentropic flow from the combustion chamber to the crankcase through an effective leakage area.

If the values of the masses and specific internal energies of both zones  $m_b$ ,  $m_u$ ,  $u_b$  and  $u_u$  are known, it is possible to calculate their derivatives since the rest of the thermodynamic variables are known:  $T_b$  and  $T_u$  can be calculated using the energy state equation, the pressure and its derivative are experimental data, the volume and its derivative depend on the angle.

The denominator of Eq. (3) never takes values close to zero even if the burned or unburned masses are small or null. This is a great advantage in the equations integration process close to combustion start and end. In Eq. (6), when  $m_b$  is very small ( $m_b/(m_u + m_b) < 10^{-5}$ ), it is assumed that the mass burned temperature is the adiabatic flame temperature.

The four Eqs. (3) (4) (5) and (6) can be jointly integrated together by numerical methods. In this case, the Runge Kutta method of order 4 with an adaptive step corrected with an order 5 is used. The experimental pressure signal filtering with splines, see Section 2, allows obtaining  $dp/dt$  from the experimental data with an acceptable level of noise to be used in the differential equations numerical integration.

The heat flow to the walls of the combustion chamber is calculated by using the film coefficient calculated with a modified Woschni correlation [37] where the density, viscosity and thermal conductivity are dependent of the mean composition, pressure and temperature, Eq. (7). The mean composition in the cylinder depends on the fuel used in each test point, the fuel equivalence ratio, and the burned mass fraction.

$$\mathbf{h} = \mathbf{Kw} \frac{\kappa}{\mu^{0.8}} 0.035 \mathbf{D}_p^{-0.2} \left[ \rho \left( 2.28 \mathbf{c}_m + 0.00324 \frac{\mathbf{V}_D T_{ac}}{\mathbf{P}_{ac} \mathbf{V}_{ac}} (\mathbf{p} - \mathbf{p}_m) \right) \right]^{0.8} \quad (7)$$

This film coefficient is used to calculate the total heat flow using the mass average temperature of the gases, but it cannot be used to calculate the wall heat transfer of each zone. The total heat flow is divided into two parts, one for the burned zone and the other for the unburned, these parts are proportional to the gas-wall temperature difference and fraction of volume of each zone.

The volume is taken and not the area because it is expected that volumes and areas are proportional since the piston cylinder head distance is much less than the piston diameter.

In Eq. (7),  $Kw$  is an adjustment coefficient with a value fixed to 0.8 by the genetic algorithm in order to obtain the cycle averaged final fraction of mass burned of  $1 \pm 0.05$  in all test points.

**Table 1**  
Expressions for the calculation of geometric variables.

Interval $\theta_{ini} \Rightarrow \theta_{fin}$	Flame front area $A_f$	Mass burned volume $V_b$	Perimeter $P_f$	Piston area projected of the unburned mass zone
$0 \Rightarrow \theta_1$ $\theta_2 \Rightarrow \theta_3$	0	$V_B(R_f \sin(\theta_{fin})) - V_B(R_f \sin(\theta_{ini}))$	0	0
$\theta_1 \Rightarrow \theta_2$ $\theta_3 \Rightarrow \theta_4$	$2\pi R_f^2 [-\cos(\theta)]_{\theta_{ini}}^{\theta_{fin}}$	$\pi R_f^3 [\frac{\cos^3(\theta)}{3} - \cos(\theta)]_{\theta_{ini}}^{\theta_{fin}}$	$2\pi R_f (\sin(\theta_{fin}) + \sin(\theta_{ini}))$	$\pi R_f^2 [\sin^2(\theta_{fin}) - \sin^2(\theta_{ini})]$
$\theta_5 \Rightarrow \theta_6$	$2\pi R_f^2 [-\cos(\theta)]_{\theta_{ini}}^{\theta_{fin}}$	$\pi R_f^3 [\frac{\cos^3(\theta)}{3} - \cos(\theta)]_{\theta_{ini}}^{\theta_{fin}}$	$2\pi V_B(R_f \sin(\theta_{fin}) + R_f \sin(\theta_{ini}))$	0
$\theta_4 \Rightarrow \theta_5$	0	$\frac{\pi D_c^2}{4} R_f [-\cos(\theta)]_{\theta_{ini}}^{\theta_{fin}}$	0	0

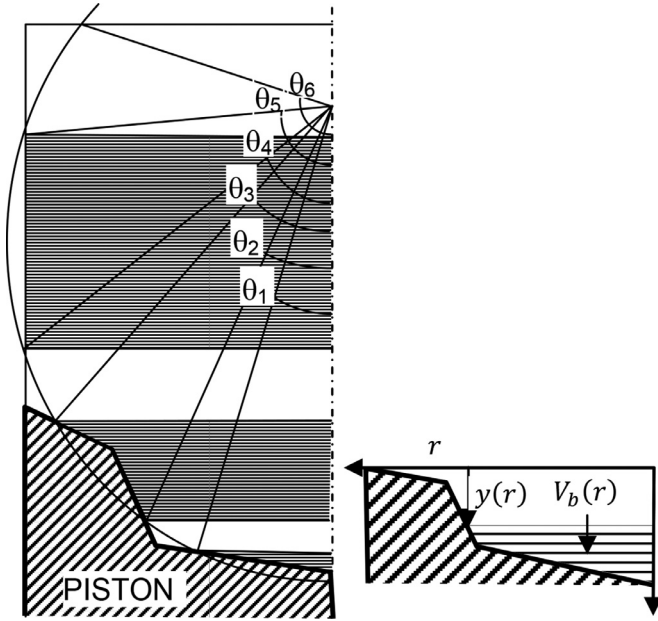


**Fig. 4.** Geometric model description.

Because there is not valve overlap, the mass of residuals for each test point is calculated assuming that the combustion chamber volume at the TDC is full of combustion products at experimental exhaust pressure and temperature.

### 3.2. Geometric model

The flame front shape in an ICE combustion chamber has different forms in each cycle due to turbulence, but the average of several cycles flame front geometries is almost spherical [38]. Under the hypothesis of the spherical flame front, a geometric model was developed in such a way that allows calculating the volume and area of a sphere of known radius  $R_f$ , centered at the spark plug position and that interferes with the surfaces of the combustion chamber.

The geometric model is based on the following: The spark plug is placed at the cylinder axis, at a given distance from the flat cylinder head; the piston surface has axial symmetry; and its highest point is in the maximum radius  $r$  position, see Fig. 4.

The piston bowl is parameterized by means of a function,  $y(r)$ , from which it is possible to calculate the bowl volume,  $V_b(r)$ , delimited between a circle of radius  $r$ , placed at a depth  $y(r)$ , and the piston surface.

At a certain flame front position  $R_f$ , once the six angles  $\theta_i$ , represented in Fig. 4 are determined, the burned mass volume  $V_b$ , the flame front area  $A_f$ , and the perimeter of the flame front touching the combustion walls  $P_f$ , are calculated with the expressions presented in Table 1.

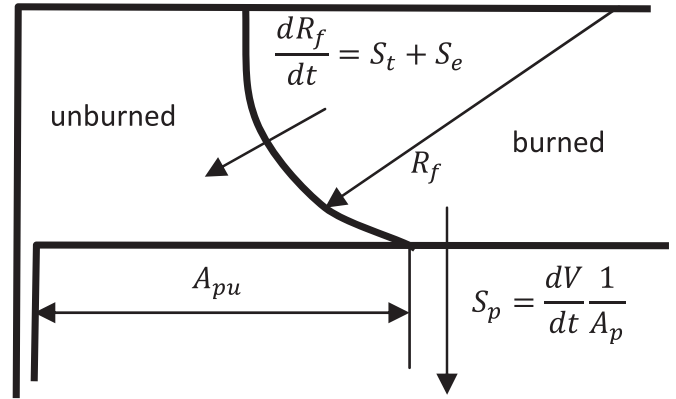


**Fig. 5.** Geometric approach for determining the flame front speed.

### 3.3. Expansion speed

In the combustion process of an internal combustion engine, the dimensions of the enclosure where the process is developed are of the same order of the integral scale size [10,14,16], so the chamber walls affect very much turbulence. Therefore, the turbulent combustion speed  $S_t$  with wall effects is different from the one developed in an open space (free field,  $S_{t\infty}$ ).

In a combustion confined in a volume, the burned products expansion produces a compression of the unburnt products and a displacement of them outwards from the ignition point. In the case of the combustion in a spherical bomb without initial turbulence, this displacement does not generate shear forces in the fluid since it is symmetrical. However, in more complex geometries such as in ICE, a relative motion with respect to the combustion chamber walls appears in the unburned fluid, due to the expansion speed, that can produce shear forces and generates turbulence, affecting the turbulent combustion speed.

The expansion speed depends strongly on the unburned and burned volumes ratio, being normally bigger at the beginning of combustion and decreasing during the combustion process. In this work, we propose that the turbulent combustion speed in a confined volume depends on the relative position of the flame front inside the combustion chamber through the expansion speed, the amount of turbulence intensity generated by  $S_e$  is proportional to the perimeter of the flame front area that wets the combustion chamber walls,  $P_f$ .

The flame front speed,  $dR_f/dt$ , is the sum of both expansion and turbulent combustion speeds, Fig. 5. As the flame front speed and the turbulent combustion speed are uniform at all the points of the flame front surface, then the expansion speed is also uniform.

The expansion speed has the following expression, see [36].

$$S_e = \frac{1}{A_f} \left( \frac{A_{pu}}{A_p} \frac{dV}{dt} + v_u \dot{m}_{bb} \right) + \frac{m_u}{pA_f} \left( \frac{dp}{dt} \frac{v_u}{\gamma_u} - \frac{\gamma_u - 1}{\gamma_u} \dot{q}_u \right) \quad (8)$$

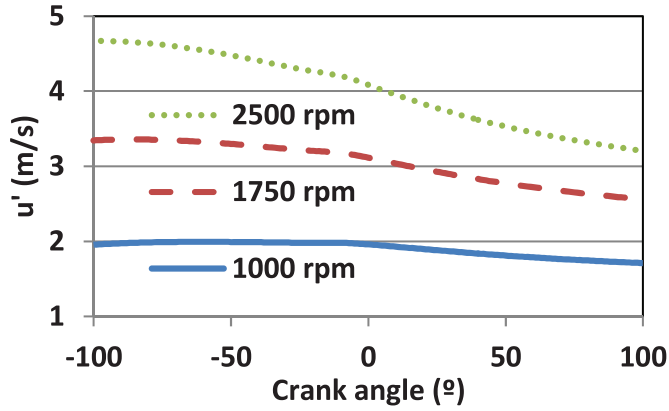


Fig. 6. Turbulent intensity  $u'$  versus crank angle calculated with AVL-BOOST 1D model in motored conditions, for the tested engine at 1000, 1750 and 2500 rpm.

It can be seen that the expansion speed is the sum of four terms. The first term is due to the piston movement through  $dV/dt$ . The second term is due to the blowby flow leakage calculated as the product of the blowby mass flow by the specific volume of the unburned mass  $v_u$ . The third term is due to the pressure variation  $dp/dt$ . And the fourth term is due to the heat transfer to the walls of the unburned mass zones,  $\dot{q}_u$ . Then the expansion speed  $S_e$  can be calculated from the thermodynamic model results.

### 3.4. Turbulence variables

It is commonly accepted [4] that the ratio of turbulent to laminar speeds  $S_t/S_l$  depends mainly on the ratio of the turbulence intensity to laminar combustion speed,  $u'/S_l$ .

The turbulence level in the combustion chamber of an ICE at the beginning of the combustion process is a result of the intake process and the piston movement. In this work, the mean turbulence intensity  $u'$  is calculated with a turbulence model *Open Chamber Gas Engine* [39]. The model assumes that the turbulence intensity is uniform in the combustion chamber, and is due to the sum of two terms, the swirl and squish flows. The squish flow is generated by the piston movement that induces a displacement of mass between the volume above the head of the piston and the one above the bowl. The variation of the swirl flow is due to the variation of the angular momentum of the mass inside the chamber and to the friction with the walls. The turbulence dissipation rate is calculated with a k-epsilon model. The initial conditions of turbulence and the speed of rotation of the air when the intake valve is closed depend on the air intake speed and the geometry of the intake ducts.

The model has been used in AVL BOOST 1D software under motored engine conditions to simulate the flow during intake and closed valve cycle. The piston geometry has been implemented in the engine model used in AVL BOOST. Figure 6 shows the results of the turbulent intensity  $u'$  versus the crank angle for three engine speeds.

In the turbulence model, the turbulence integral scale  $L_t$ , is assumed to be the distance from the piston to the cylinder head [10,14,16]. When this length is used in the analysis of results, it is calculated at the position of the flame front.

### 3.5. Laminar combustion speed and diffusive properties

The corresponding laminar combustion speed  $S_l$  at each angle is calculated using the expressions proposed by Bougrine [6] for  $\text{CH}_4$  and  $\text{H}_2$  mixtures. This expression depends on the composition, equivalence ratio, pressure, temperature and residual gas fraction.

The thermal conductivity,  $\kappa$ , for both pure substance and unburned products mixtures are calculated with the expression proposed by Wassiljewa [40] with the modifications of Mason and Saxena [41] according to [42]. For the heat capacities, the correlations proposed by [43] have been used.

The thermal diffusivity values,  $\alpha$ , are calculated using the thermal conductivity and heat capacities values. The density values are calculated under the hypothesis of ideal gas.

For the calculation of the pure substance viscosities, the corresponding states method has been used. The viscosity in mixtures has been calculated with the Wilke method [44], given in the same source [42].

The mass diffusivity in mixtures is calculated with the Blanc's law presented in [42] once the mass diffusivities of binary mixtures are calculated through the theoretical expression given in the same book.

### 3.6. Combustion instabilities variables

As indicated in the introduction, it is possible that instabilities affect the combustion process. An instability with a unit amplitude at the time instant  $t=0$  has an amplitude  $e^{\omega t}$  after an elapsed time  $t$ . The amplitude growth rate  $\omega$  for a given wavelength  $\lambda$  has, according to the hydrodynamic theory – multiscale analysis [8], the approximate expression:

$$\omega(\lambda) = \omega_{DL} \mathbf{S}_1 \frac{2\pi}{\lambda} - \mathcal{L} \frac{\sigma(1 + \omega_{DL})(\sigma + \omega_{DL})}{\sigma + (\sigma + 1)\omega_{DL}} \mathbf{S}_1 \left( \frac{2\pi}{\lambda} \right)^2 \quad (9)$$

Where the Markstein length  $\mathcal{L}$  is calculated using the expression given by [45]

$$\mathcal{L} = \delta_l \left[ \frac{\sigma \ln \sigma}{\sigma - 1} + \frac{\beta(\mathbf{Le}_{eff} - 1)}{2(\sigma - 1)} \int_1^\sigma \frac{\ln \mathbf{x}}{\mathbf{x} - 1} d\mathbf{x} \right] \quad (10)$$

The wave growth rate depends on the pressure, temperature and composition parameters through Zel'dovich number  $\beta$ , laminar combustion speed  $S_l$ , effective Lewis number  $\mathbf{Le}_{eff}$ , thickness of flame front  $\delta_l$ , density ratio  $\sigma$ ; and on  $\omega_{DL} = (\sqrt{(\sigma^3 + \sigma^2 - \sigma) - \sigma})/(\sigma + 1)$ , that only depends on the density ratio  $\sigma$ .

When  $\omega(\lambda) > 0$  the instability grows, while when  $\omega(\lambda) < 0$  the system is stable for a perturbation of wavelength  $\lambda$ . The first term on the right hand of Eq. (9) is always positive since  $\sigma > 1$ . The second term sign depends on the  $\mathcal{L}$  sign. This term can be negative, if  $\mathbf{Le}_{eff}$  is below a certain value; in that case, the instabilities grow for all the wavelength values.

Figure 7 shows the amplitude growth rate,  $\omega(\lambda)$  of an instability, as a function of the wavelength non-dimensionalized with the integral length scale,  $\lambda/L_t$ , for natural gas with fuel air-equivalence ratio  $\phi=0.7-1.0$  (continuous line) and for hydrogen with  $\phi=0.4-0.7$  (dashed line), for the more extreme temperature and pressure, corresponding to the points:  $R_f/R_p = 0.2$  and 1000 rpm and  $R_f/R_p=0.8$  and 2500 rpm. The growth rate value increases with the fuel air equivalence ratio.

It can be seen that the amplitude growth rate for hydrogen is positive for all wavelengths. In the case of natural gas, for wavelength between  $\lambda/L_t=0.1$  to 1.0, the growth rate is positive and lower than the ones of hydrogen. There is a wide range of wavelengths below the characteristic dimension of the phenomenon  $L_t$  that will grow the instability amplitude causing the deformation of the flame front. It can be concluded that for all the test points there will be increasing instabilities of wavelength smaller than the size of the wrinkles generated by the turbulence,  $L_t$ .

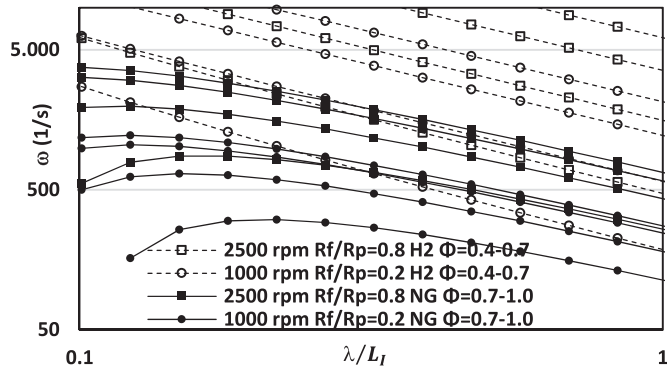


Fig. 7. Growth rate  $\omega(\lambda)$ , versus dimensionless wavelength  $\lambda/L_f$ , for natural gas with fuel air-equivalence ratio  $\phi=0.7, 0.8, 0.9$  and  $1.0$  (continuous line) and for hydrogen with  $\phi=0.4, 0.5, 0.6$  and  $0.7$  (dashed line), for the more extreme temperature and pressure thermodynamic conditions points:  $R_f/R_p = 0.2$  and  $1000$  rpm and  $R_f/R_p=0.8$  and  $2500$  rpm. The growth rate value increases with the fuel air equivalence ratio.

## 4. Results and discussion

### 4.1. Experimental values of turbulent combustion speed, $S_t$

Figure 8 presents an example of the results of the instantaneous turbulent combustion speed of 200 consecutive cycles versus the dimensionless flame front radius,  $R_f/R_p$  (left), and versus the crank angle (right), obtained for test conditions of  $1750$  rpm and  $50\%$  H<sub>2</sub>. The thick lines represent the cycle average turbulent combustion speed for each radius,  $S_t$  (left axis), while the dashed lines represent the laminar combustion speed  $S_l$  (right axis). Notice that the laminar speed varies between  $0.5$  and  $0.6$  m/s. At each flame front position, the instantaneous turbulent combustion speed of each engine cycle fluctuates around the mean value. At the combustion beginning,  $R_f/R_p < 0.1$ , the calculated  $S_t$  cannot be considered reliable because the difference between the pressure signal with and without combustion is of the same order than the signal noise.

Although the flame front radius could be higher than the piston radius, this would correspond to a piston position well down along the expansion stroke, not relevant for combustion analysis in this work since other effects such as quenching would come into play.

It is possible to see in Fig. 8 that for  $R_f/R_p \approx 0.6$  ( $24$  mm) the combustion speed slope varies sharply, which happens when the flame front leaves the deepest part of the piston bowl. The same trend can be seen with less sharpness at  $R_f/R_p=0.25$ , when the flame front starts touching the piston (see Fig. 2 for reference).

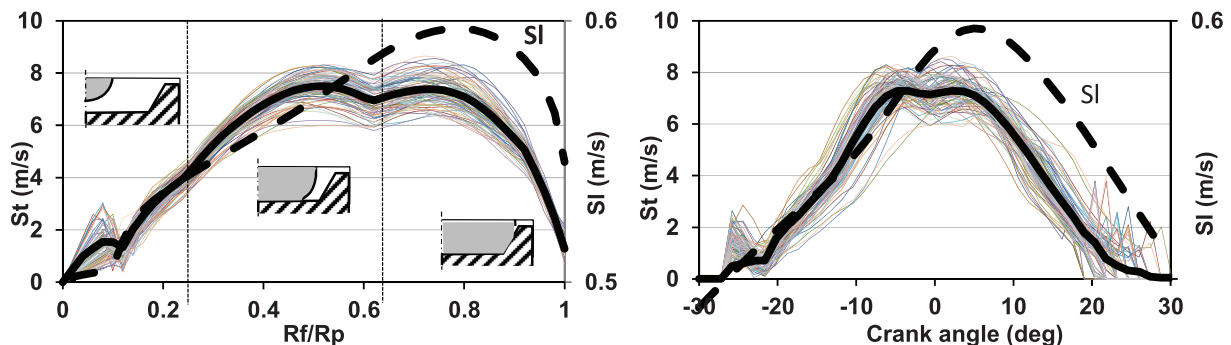


Fig. 8. Plots of instantaneous turbulent combustion speed  $S_t$  versus dimensionless flame front radius  $R_f/R_p$  (left) and versus the crank angle (right) for 100 consecutive cycles. Engine speed  $1750$  rpm,  $50\%$  H<sub>2</sub>. The thick continuous line represents the average turbulent combustion speed  $S_t$  (left axis) and the dashed line the laminar combustion speed  $S_l$  (right axis).

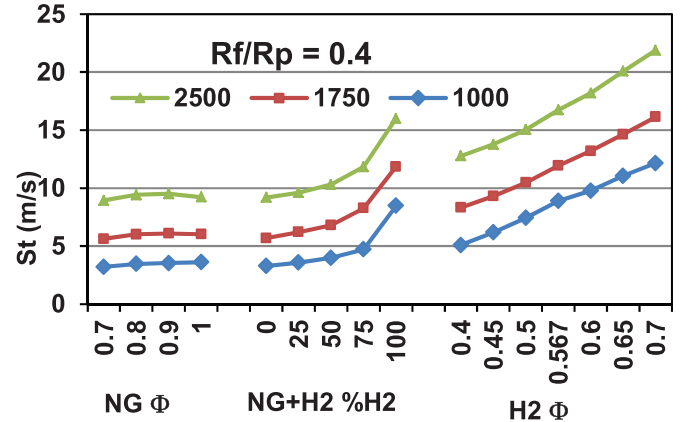


Fig. 9. Cycle averaged turbulent combustion speed  $S_t$  versus fuel type, and engine speed (rpm) as parameter. Flame front position  $R_f/R_p=0.4$ . The equivalence ratio for NGH<sub>2</sub> mixtures can be seen in Fig. 3.

The combustion process develops with a combustion speed higher than the laminar combustion speed even from the first moments. After having touched the piston, the velocity stabilizes between  $R_f/R_p=0.4$  and  $0.6$  in the intermediate phase, a situation that [29] calls turbulent front fully developed. Finally, the turbulent combustion speed decreases appreciably due to the wall proximity, above  $R_f/R_p=0.9$ . The behavior of lines for each NG+H<sub>2</sub> mixture is similar to the seen in Fig. 8, although the higher the hydrogen content in the mixture, the higher the combustion speed.

In Fig. 9 the averaged turbulent combustion speed at the position  $R_f/R_p=0.4$  is presented for all experimental tests (different fuels, equivalence ratios, hydrogen percentages, engine rpms). A remarkable influence of the engine speed and laminar combustion speed (through equivalence ratio and hydrogen percentage) on the turbulent combustion speed is observed.

### 4.2. Correlation of the turbulent combustion speed

Four positions of the flame front that characterize three combustion stages: initial ( $R_f/R_p=0.2$ ), developed ( $R_f/R_p=0.4$  and  $0.6$ ), and final ( $R_f/R_p=0.8$ ) have been chosen. All data are presented in [36].

The experimental results of  $S_t$  obtained with the thermodynamic and geometric model from pressure measurements can be adjusted with an expression of the type of  $S_t/S_l - 1 = K_0(u'/S_l)^{K_1}$  used by several authors [3,4,46–48], by using a linear regression to calculate the values of constant  $K_0$  and exponent  $K_1$ . In literature, for flames in a free field, the values of  $K_1$  is usually between  $0.5$



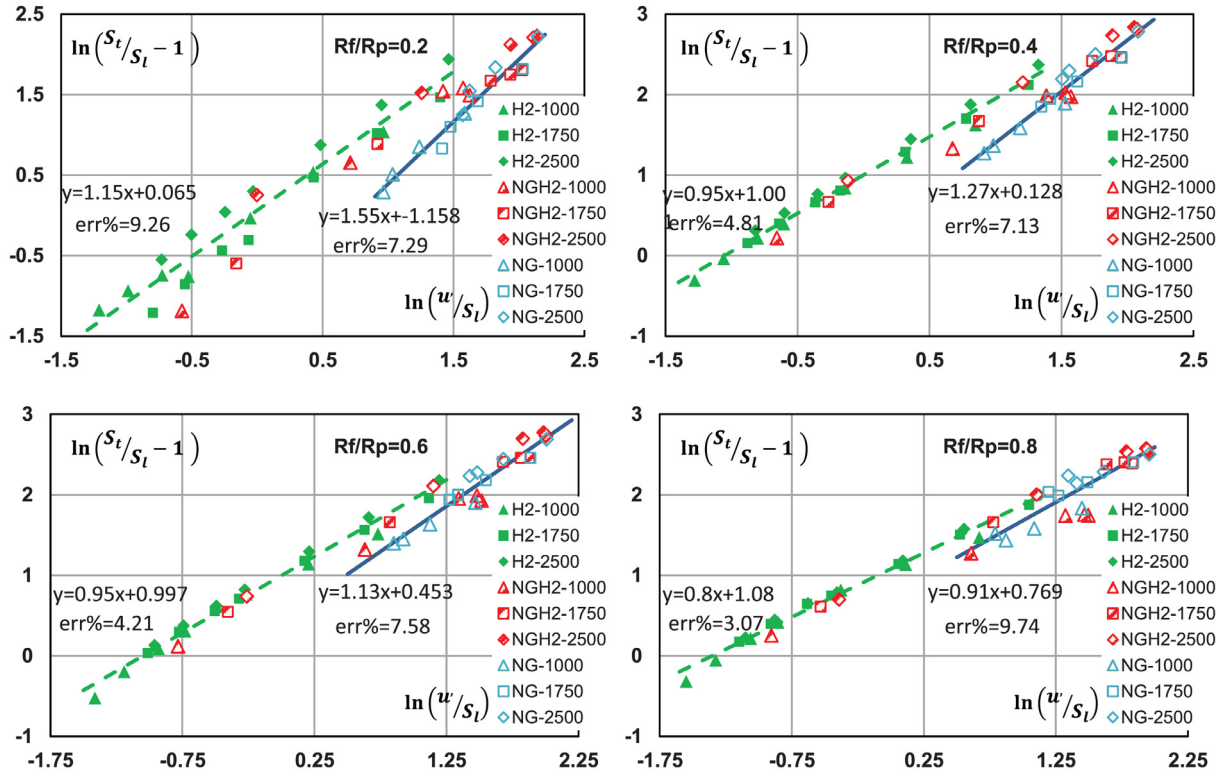


Fig. 10.  $\ln(S_t/S_l - 1)$  versus  $\ln(u'/S_l)$  for the flame front position  $R_f/R_p = 0.2, 0.4, 0.6$  and  $0.8$ . All the fuel air equivalence ratios, mixing proportions and engine speeds are included. Each color is for one type of fuel: H2, NG and NGH2 mixes.

and 1 [4]. In Fig. 10, the experimental results of  $y = \ln(S_t/S_l - 1)$  versus  $x = \ln(u'/S_l)$  are presented, showing the values of  $K_1$  and  $\ln(K_0)$  in the correlation lines, and the average relative error.

The solid lines represent the linear fit for the natural gas (blue) cases, while dash lines are for hydrogen (green) cases. The dependence of  $S_t$  with  $u'$  is different for each fuel and the four flame front position. The NGH2 mixtures present an intermediate behavior (red points).

Looking at Fig. 10, it can be concluded that the ratio  $S_t/S_l$  depends on the turbulence intensity, but there are some other variables that influence and make the slopes different for NG and H2.

To account for the fuel influence, a second parameter is introduced. This relates a property of the turbulent combustion with another of the laminar combustion process is  $L_f/\delta_l$ . This parameter is usually used in expressions to determine  $S_t/S_l$ , or sometimes through Damköhler or Reynolds number [3,7,49,50], in the way:

$$\begin{aligned} S_t/S_l - 1 &= K_0 (u'/S_l)^{K_1} (L_f/\delta_l)^{K_2} = K_0 (u'/S_l)^{K_1+K_2} Da^{K_2} \\ &= K_0 (u'/S_l)^{K_1-K_2} Re_{L_f}^{K_2} \end{aligned} \quad (11)$$

where  $\delta_l = \alpha/S_l$  when the Damköhler number is used or  $\delta_l = \nu/S_l$  when the Reynolds number is used. This introduced parameter relates the size of the largest eddies with the thickness of the laminar flame front. The larger the integral scale and the smaller the thickness of the flame front, the higher the turbulence influence on the value of  $S_t/S_l$ . Hereinafter the thermal flame thickness is used  $\delta_l = \alpha/S_l$ .

Figure 11 shows the results of the obtained adjustments of  $(S_t/S_l - 1)$  with a power function dependent on two dimensionless variables, as Eq. (11), for the flame front position  $R_f/R_p=0.4$ . The relative error and the parameters of the obtained adjustment are presented in the figure. Two different trend lines can be seen

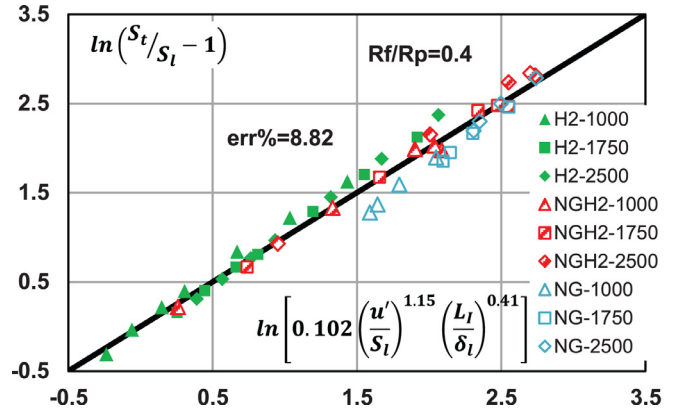


Fig. 11. Experimental data of  $\ln(S_t/S_l - 1)$  versus values obtained from the adjustment expression  $\ln[K_0 (u'/S_l)^{K_1} (L_f/\delta_l)^{K_2}]$ , for  $R_f/R_p=0.4$ . The adjustments include all the H2, NG and NGH2 fuels, at 1000, 1750 and 2500 rpm engine speeds.

for H2 and NG. Similar results are obtained for the other positions of the flame front.

Figure 7 shows that in all test conditions the instabilities grow if their wavelengths are smaller than the integral scale. Assuming the hypothesis that these instabilities cause a thickening of the flame front, the instabilities would represent a change in the influence of the turbulence on  $S_t/S_l$  value.

The amplitude of the instabilities,  $A$ , depends on the rate of growth,  $\omega$ , but also on the time elapsed since the instability had a certain initial amplitude  $A_0$ . Choosing a characteristic time as the time that the flame front takes to travel the integral length scale eddy,  $L_f/S_l$ , an initial amplitude equal to the thickness of the flame front,  $\delta_l$ , and an instability wavelength equal to the integral scale,  $L_f$ , the amplitude of the instability would have the expression of

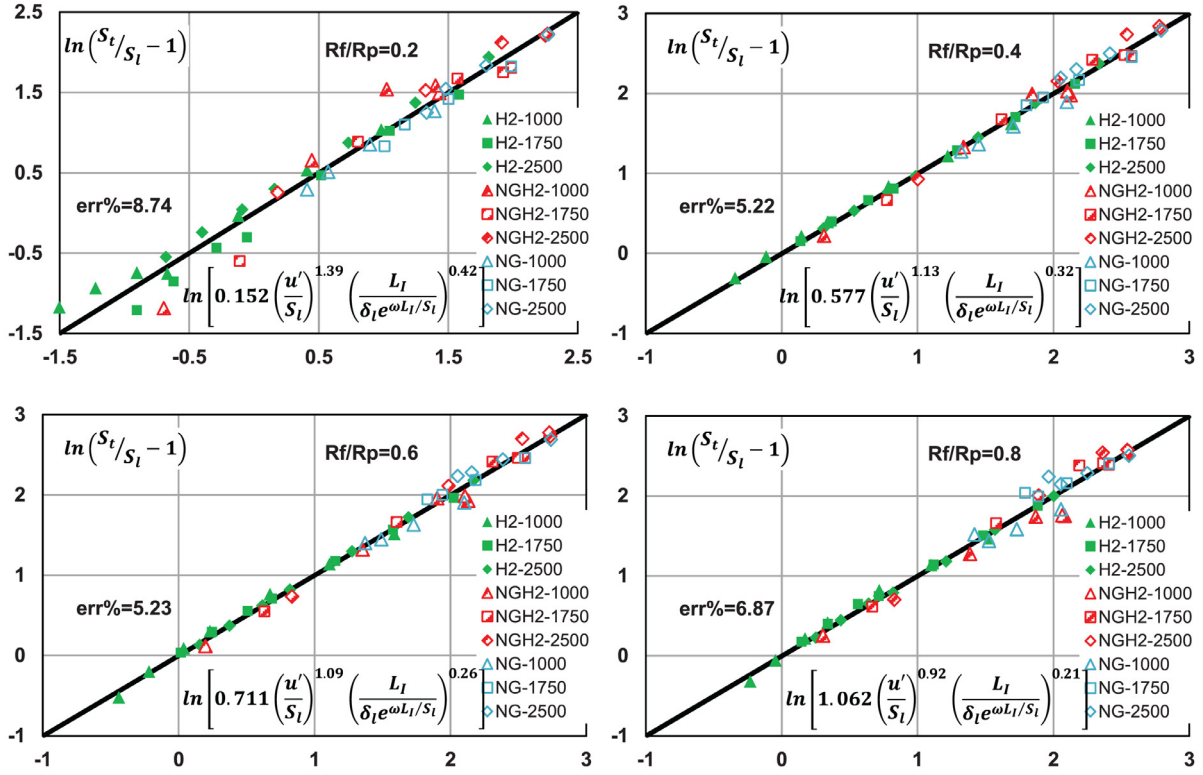


Fig. 12. Experimental data of  $\ln(S_t/S_l - 1)$  versus values obtained from the adjustment expression  $\ln[K_0(u'/S_l)^{K_1} (L_l/(\delta_l e^{\omega L_l/S_l}))^{K_2}]$ , for four flame front positions. The adjustments include all the H2, NG and NGH2 fuels, at 1000, 1750 and 2500 rpm engine speeds.

Eq. (12):

$$\begin{aligned} \mathbf{A} &= \mathbf{A}_0 e^{\omega t} = \delta_l e^{\omega \frac{L_l}{S_l}} \\ &= \delta_l \exp\left(2\pi\omega_{DL} - \mathcal{L} \frac{\sigma(1 + \omega_{DL})(\sigma + \omega_{DL})4\pi^2}{\sigma + (\sigma + 1)\omega_{DL}} \frac{4\pi^2}{L_l}\right) \end{aligned} \quad (12)$$

This increased thickness of the flame front,  $\delta_l e^{\omega \frac{L_l}{S_l}}$ , can replace the laminar flame front thickness in Eq.(11) and be used to obtain an expression of  $S_t/S_l$  of the form of Eq. (13):

$$\frac{S_t}{S_l} - 1 = K_0 \left(\frac{u'}{S_l}\right)^{K_1} \left(\frac{L_l}{\delta_l e^{\omega L_l/S_l}}\right)^{K_2} \quad (13)$$

Figure 12 shows the results of the obtained adjustments of  $(S_t/S_l - 1)$  with a power function dependent on two dimensionless variables, as Eq. (13), for the four flame front positions. The relative error and the parameters of the obtained adjustment are presented in the figure.

The results of Fig. 12 in  $R_f/R_p=0.4$  show a better adjustment than in Fig. 11, reflected in the improvement of both the relative mean error of 8.82% to 5.22%, and in the aligned position of the points for H2 and NG.

The positive value of the exponent of  $L_l/(\delta_l e^{\omega L_l/S_l})$  implies that the higher the amplitude of the instabilities for the characteristic time,  $\delta_l e^{\omega L_l/S_l}$ , the lower the  $S_t/S_l$  ratio. This is what has caused the prediction of  $S_t/S_l$  in Fig. 11 of the NG to decrease and those of hydrogen to increase, so that they approach more the experimental data. This is the same for the four values of the flame front radius.

This behavior is better understood by observing Fig. 13 where the growth rate,  $\omega$ , and the multiplier of the flame front thickness,  $e^{\omega L_l/S_l}$ , values are represented for NG an H2, at  $R_f/R_p = 0.4$  and 1750 rpm. The growth rate  $\omega$  is higher for H2 than for NG, however the multiplier value of the initial amplitude reached at

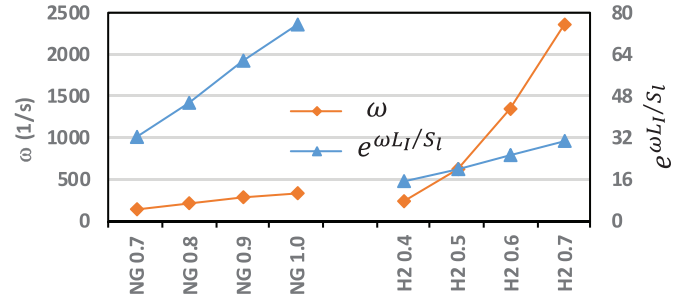


Fig. 13. Growth rate,  $\omega$ , and multiplier of the flame front thickness,  $e^{\omega L_l/S_l}$ , for NG and H2, at flame front position  $R_f/R_p=0.4$  and 1750 rpm.

the time interval in which an eddy is burned,  $\delta_l e^{\omega L_l/S_l}$ , is bigger for NG, because of the lower value of  $S_l$ .

The adjustment coefficients  $K_1$  of Fig. 11 and  $K_0, K_1$  and  $K_2$  of Fig. 12 are shown in Table 2. It is observed that the  $K_1$  exponent of  $u'/S_l$  and  $K_2$  exponent of  $L_l/(\delta_l e^{\omega L_l/S_l})$  decreases as the radius of the flame front increases. On the other hand, the coefficient  $K_0$  increases with the radius of the flame front.

#### 4.3. Unified correlation of combustion speed for all flame front positions

From Fig. 12 and Table 2, it can be concluded that, the ratio  $S_t/S_l$  depends on the radius of the flame front in some way. The most probable reasons for this difference can be attributed to the confined and transitory nature of the combustion process in the engine.

In the flame front, a relative movement  $S_e$  Eq. (8) between unburnt products and walls exists, so shear forces generate additional turbulence near the wall. To quantify this effect a new term is pro-

**Table 2**  
Adjustment coefficients  $K_1$  of Fig. 10, and  $K_0$ ,  $K_1$  and  $K_2$  of Fig. 12.

$R_f/R_p$	Adjustment coefficients Fig. 10		Adjustment coefficients Fig. 12			
	$K_{1H2}$	$K_{1NG}$	$K_0$	$K_1$	$K_2$	Relative error (%)
0.2	1.15	1.55	0.15	1.39	0.42	8.74
0.4	0.95	1.27	0.58	1.13	0.32	5.22
0.6	0.95	1.13	0.71	1.09	0.26	5.23
0.8	0.8	0.91	1.06	0.92	0.21	6.87

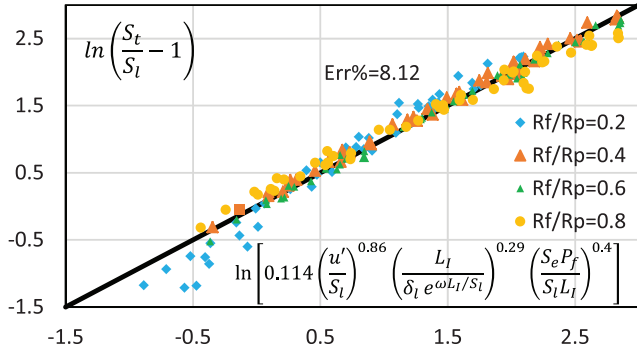


**Fig. 14.** Experimental data of  $\ln(S_t/S_l - 1)$  versus values obtained from the correlation expression of Eq. (14). The plot includes all experimental points with H2, NG and NGH2 fuels, at 1000, 1750 and 2500 rpm engine speeds and the four flame front positions.

posed which is the product of the speed of the unburned products in the flame front,  $S_e$ , and the perimeter  $P_f$  of the flame front that wet the walls, since the process of combustion will be affected by the turbulence generated in this area. To do that in a dimensionless way, this product is divided by the laminar combustion speed  $S_l$  and the flame front height that in this case coincides with the  $L_l$  (see the end of Section 3.4). The height of the flame front quantifies the relative importance of this effect on the whole flame front, since the bigger this distance, the smaller the influence of the increase of the  $S_t$  near the walls on the average  $S_t$  in the whole flame front area.

This additional term will reduce the  $S_t/S_l$  in the early stages of combustion because although  $S_e$  is high, the perimeter is small. In addition, when the combustion is finishing, that is, when the unburned mass is very small, the expansion speed is practically null, so that the combustion speed will end at values close to the  $S_l$ .

Figure 14 represents the  $(S_t/S_l - 1)$  adjustment for all the flame front radii and all fuels considered using the expression:

$$\frac{S_t}{S_l} - 1 = K_0 \left( \frac{u'}{S_l} \right)^{K_1} \left( \frac{L_l}{\delta_l e^{\omega L_l / S_l}} \right)^{K_2} \left( \frac{S_e P_f}{S_l L_l} \right)^{K_3} \quad (14)$$

It is important to notice that in the unified correlation the exponent of the term  $u'/S_l$  takes values less than 1, in agreement with other published results (values between 0.5 and 1.0).

An expression of the free field turbulent combustion correlation can be written in the form:

$$\frac{S_{t\infty}}{S_l} - 1 = K_{off} \left( \frac{u'}{S_l} \right)^{0.86} \left( \frac{L_l}{\delta_l e^{\omega L_l / S_l}} \right)^{0.29} \quad (15)$$

where  $S_{t\infty}$  is the turbulent combustion speed in a free field. This expression can be corrected with the term associated to the expansion velocity, to provide the value of the confined turbulent combustion speed in the following form, which constitutes a unified

correlation for all experimental conditions:

$$\frac{S_t}{S_l} - 1 = \left( \frac{S_{t\infty}}{S_l} - 1 \right) K_{ocf} \left( \frac{S_e P_f}{S_l L_l} \right)^{0.4} \quad (16)$$

where  $K_0 = K_{off} K_{ocf}$ .

Eq. (15) can be written as follow:

$$\frac{S_{t\infty}}{S_l} - 1 = K_{off} \left( \frac{u'}{S_l} \right)^{1.15} Da^{0.29}$$

Where in the Damköhler number  $\delta_l$  is multiplied by  $e^{\omega L_l / S_l}$  thus providing the widened thickness. This expression is similar to the one proposed by Wallesten et al. [51],  $S_{t\infty}/S_l - 1 = A (u'/S_l) Da^{0.25}$ , where the exponents values change from 1 to 1.15 and from 0.25 to 0.29.

If  $Pr = 1$ , in this case  $\delta_l = \nu/S_l$ , Eq. (15) can be written as:

$$\frac{S_{t\infty}}{S_l} - 1 = K_{off} \left( \frac{u'}{S_l} \right)^{0.57} Re_{L_l}^{0.29}$$

Where  $L_l$  used in  $Re_{L_l}$  is divided by  $e^{\omega L_l / S_l}$ . Comparing with the expression proposed by Gülder [3] for wrinkled flame regime,  $S_{t\infty}/S_l - 1 = 0.6 (u'/S_l)^{0.5} Re_{L_l}^{0.25}$ , the exponents change from 0.5 to 0.57 and from 0.25 to 0.29. The value of the coefficient  $K_{off}$  in Gülder [3] is 0.6, so if this value is accepted, the value of the coefficient  $K_{ocf}$  would be 0.19.

## 5. Correlation of combustion speed to be used in predictive models

If Eq. (16) is to be used in a predictive model for calculating the pressure from the combustion rate, it has the problem that the expression of Eq. (8) of expansion speed include the variable  $dp/dt$ . In a predictive model  $dp/dt$  depends on  $dm_b/dt = S_t A_f \rho_u$ , which depends in turn on  $S_t$ . For that reason, it is more convenient to have an explicit expression of  $S_e$ .

If the same properties of the burned and unburned zones are considered, the expression of the expansion speed of Eq. (8) can be modified (see [36]) to obtain Eq. (17):

$$S_e = \frac{1}{A_f} \left[ \frac{dV}{dt} \left( \frac{A_{pu}}{A_p} - \frac{V_u}{V} \right) + v_u \dot{m}_{bb} \right] + S_t \left( \frac{(\gamma - 1) m_u H_p}{\gamma p V} \right) + \frac{(\gamma - 1)}{\gamma p A_f} \left( \dot{Q}_w \frac{V_u}{V} - \dot{Q}_u \right) \quad (17)$$

The terms due to the piston movement,  $dV/dt$ , blow-by flow,  $\dot{m}_{bb}$ , and heat transfer,  $\dot{Q}_w$  and  $\dot{Q}_u$ , can be neglected, since piston speed near TDC is small and the other two terms take values ten times smaller than the term with  $S_t$ .

$S_t$  can be estimated by  $\sqrt{u' S_l}$  that presents tendencies similar to  $S_t$  and the same units.

With these considerations, the resulting estimated expansion velocity  $S_e^\#$  is:

$$S_e^\# = \frac{(\gamma - 1) m_u H_p}{\gamma p V} \sqrt{u' S_l} \quad (18)$$

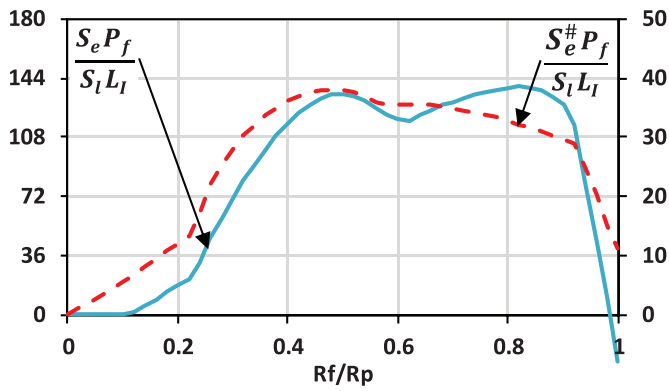


Fig. 15. Comparison of dimensionless number for the correction of free field expression using the expansion speeds  $S_e$  (continuous line, left axis) and  $S_e^\#$  (dashed line, right axis) for 75% of H2 and 1750 rpm.

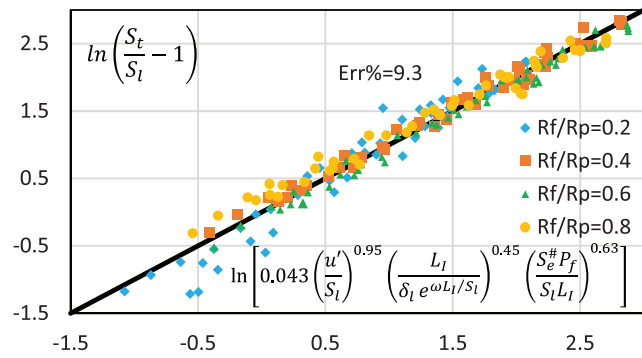


Fig. 16. Values of  $(S_t/S_l - 1)$  calculated with Eq.(14) using  $S_e^\#$  instead  $S_e$ . The plot includes all experimental points with H2, NG and NGH2 fuels, at 1000, 1750 and 2500 rpm engine speeds and the four flame front positions.

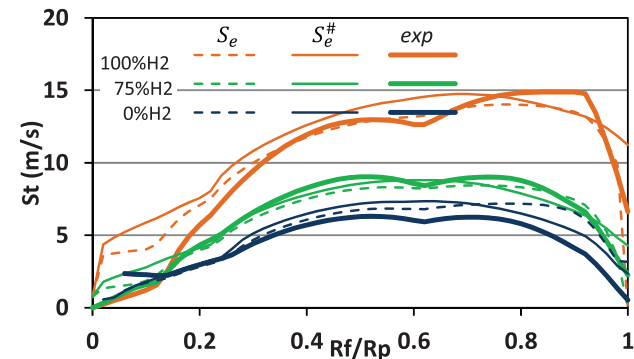


Fig. 17. Results of the turbulent combustion speed  $S_t$  calculated with the adjustment of Fig. 14, using the expansion speed  $S_e$  of Eq. (8) (dashed line) and  $S_e^\#$  of Eq.(18) (thin continuous line), and the average value of experimental  $S_t$  (thick continuous line), versus the dimensionless flame front radius, for the case of NGH2 mixtures with different H2, at 1750 rpm.

In Fig. 15, a comparison of the dimensionless number for the correction of free field expression is presented using the expansion speeds  $S_e$  and  $S_e^\#$ , for 75% of H2 and 1750 rpm, showing that they have the same trends, but different values represented in two different axes:

In Fig. 16(a) new adjustment of  $(S_t/S_l - 1)$  with the expression of Eq. (14) using  $S_e^\#$  instead  $S_e$  is showed. In this case, the relative error is 9.3%.

Figure 17 shows the values of  $S_t$  versus the dimensionless flame front radius, when  $S_t$  is calculated with the adjustment of Fig. 14 using the expansion speed  $S_e$  of Eq. (8) and calculated with the ad-

justment of Fig. 16 using  $S_e^\#$  of Eq. (18). Also the average value of experimental  $S_t$  is presented, for the case of NGH2 mixtures with different percentage of H2% at 1750 rpm.

The agreement with experimental values is considered acceptable even for the beginning and end of combustion, and not only in the range of the developed combustion.

## 6. Conclusions

The combustion diagnosis from pressure measurement in an engine and its processing with thermodynamic and geometric models provides values of the turbulent combustion speed averaged over the entire surface of the flame front. The automation of the combustion diagnosis with the use of a strategy based on genetic algorithms has allowed the processing of nearly 10,000 engine cycles, for different fuels, equivalence ratios and engine speeds. To make the analysis of the combustion process, a cycle average of the most significant variables in four positions of the flame front has been made of each engine operating point.

With the objective of developing an analytical expression of the turbulent combustion speed depending on the relevant variables of the combustion process, it has been confirmed that the main dependence of the turbulent combustion speed (normalized with the laminar combustion speed,  $S_t/S_l$ ) is on normalized flow turbulence intensity ( $u'/S_l$ ). However, different trends are observed for each fuel, hydrogen and natural gas, that are attributed to the influence of instabilities in  $S_t/S_l$ .

To take into account the interaction between instabilities and turbulence on the analytical expression, the parameter that relates the eddy size with the laminar flame front thickness,  $L_l/\delta_l$ , has been modified. The laminar flame front thickness is substituted by the instabilities amplitude,  $L_l/(\delta_l e^{\omega L_l/S_l})$ . An expression of  $S_t/S_l$  valid for natural gas and hydrogen, and also their mixtures has been obtained (Eq. (13) and Fig. 12).

As a conclusion of the obtained results, the influence of the instabilities on turbulence depends on the product of two parameters: the rate of growth of the instabilities,  $\omega$  (bigger for H2), and the time that the flame front takes to travel the integral length scale eddy,  $L_l/S_l$  (smaller for H2). According to the obtained results, the smaller the amplitude of the instabilities,  $\delta_l e^{\omega L_l/S_l}$ , the bigger  $S_t/S_l$ .

Once the influence of instabilities has been introduced into the correlation, the obtained correlation coefficients depend on the flame front position because the development of a confined combustion is highly transient. The additional turbulence generated by the shear stresses produced by the relative movement between the unburned mixture and the walls increases  $S_t$  with respect to what would be in the free field. This influence is different for each position of the flame front because the expansion speed,  $S_e$ , depends on  $S_t$  and varies as the combustion process develops. This would justify that the exponents of  $u'$  in the correlations of each flame front position are greater at the beginning of combustion.

A unified correlation considering  $S_e$ , (Eq. (14) and Fig. 14) has been obtained to predict all experimental points, independently of engine speed, fuel composition or flame front position, with an error of estimation of about 8%. Additionally, an expression of the value of the turbulent combustion speed in free field  $S_{t\infty}$ , Eq. (15), can be derived from Eq. (14). The correlation exponents obtained for free field are close to those proposed by other authors.

This unified correlation can be used in quasi-dimensional models to predict combustion in internal combustion engines. This correlation should be tested on engines with other characteristics and extend the range of operating conditions.

Possibly, the data used in this work with the biggest uncertainty is the  $u'$  value. A 0-Dimensional model has allowed an estimation of the  $u'$  for the different engine speeds. In any case, with

the hypothesis of the turbulence intensity is linear with the engine speed, as discussed in the introduction, if the value of  $u'$  would be substituted by the mean piston speed, the resulting correlation in the form of Eq. (14) would have the same exponent  $K_1$  although a different coefficient  $K_0$ .

### Declaration of Competing Interest

None.

### Acknowledgments

The authors of this work would like to thank the Spanish Ministry of Science and Innovation for the financial support of this research through the [ENE 2012-34830](#) (with FEDER funds) and the Regional Government of Castile and Leon for funding the Excellence Research Group GR203

### Mendeley data

Giménez, Blanca; Melgar, Andrés; Horrillo, Alfonso; Tinaut, Francisco (2019), "Combustion speed in ICE: thermodynamic model for combustion speed, expansion speed, data base", Mendeley Data, v1. Published: 31 Jul 2019. DOI: [10.17632/wskmmkg6rk.1](#)

### References

- [1] R. Borghi, Turbulent combustion modelling, *Prog. Energy Combust. Sci.* 4 (1988) 245–292.
- [2] Y. Liu, B. Lenze, The influence of turbulence on the burning velocity of premixed CH<sub>4</sub>-H<sub>2</sub> flames with different laminar burning velocities, *Symp. (Int.) Combust.* 22 (1988) 747–754.
- [3] Ö.L. Gülder, Turbulent premixed flame propagation models for different combustion regimes, *Symp. (Int.) Combust.* 23 (1991) 743–750.
- [4] A.N. Lipatnikov, J. Chomiak, Turbulent flame speed and thickness: phenomenology, evaluation, and application in multi-dimensional simulations, *Prog. Energy Combust. Sci.* 28 (2001) 1–74.
- [5] S. Verhelst, C. Tjoen, J. Vancoillie, J. Demuyne, A correlation for the laminar burning velocity for use in hydrogen spark ignition engine simulation, *Int. J. Hydrogen Energy* 36 (2011) 957–974.
- [6] S. Bougrine, S. Richard, A. Nicolle, D. Veynante, Numerical study of laminar flame properties of diluted methane-hydrogen-air flames at high pressure and temperature using detailed chemistry, *Int. J. Hydrogen Energy* 36 (2011) 12035–12047.
- [7] A.N. Lipatnikov, J. Chomiak, Turbulent flame speed and thickness: phenomenology, evaluation, and application in multi-dimensional simulations, *Prog. Energy Combust. Sci.* 28 (2002) 1–74.
- [8] M. Matalon, The Darrieus-Landau instability of premixed flames, *Fluid Dyn. Res.* 50 (2018) 51412.
- [9] M. Matalon, Intrinsic flame instabilities in premixed and nonpremixed combustion, *Annu. Rev. Fluid Mech.* 39 (2007) 163–191.
- [10] D.R. Lancaster, Effects of engine variables on turbulence in a spark-ignition engine, *SAE Technical Paper Series* 760159 (1976).
- [11] R.J. Tabaczynski, Turbulence and turbulent combustion in spark-ignition engines, *Prog. Energy Combust. Sci.* 2 (1976) 143–165.
- [12] E.H. James and G.G. Lucas, Turbulent flow in spark ignition engine combustion chambers, *SAE Technical Paper Series* 750885 (1975).
- [13] C. Arcoumanis, J.H. Whitelaw, Fluid mechanics of internal combustion engines—a review, *Proc. Inst. Mech. Eng. C: J. Mech. Eng. Sci.* 201 (1987) 57–74.
- [14] R.G. Prucka, T.-K. Lee, Z. Filipi, and D.N. Assanis, Turbulence Intensity calculation from cylinder pressure data in a high degree of freedom spark-ignition engine, *SAE Technical Paper Series* (2010).
- [15] J.B. Cole, M.D. Swords, Optical studies for turbulence in internal combustion engine, *Symp. (Int.) Combust.* 17 (1979) 1295–1303.
- [16] Z.S. Filipi, D.N. Assanis, The effect of the stroke-to-bore ratio on combustion, heat transfer and efficiency of a homogeneous charge spark ignition engine of given displacement, *Int. J. Engine Res.* 1 (2000) 191–208.
- [17] K.N.C. Bray, P. Libby, G. Masuya, J.B. Moss, Turbulence production in premixed turbulent flames, *Combust. Sci. Technol.* 25 (1981) 127–140.
- [18] J.B. Heywood, Combustion and its modeling in spark-ignition engines, *Int. Symp. COMODIA* 94 (1991) 1–15.
- [19] R.N. Paul, K.N.C. Bray, Study of premixed turbulent combustion including landau-darrieus instability effects, *Symp. (Int.) Combust.* 26 (1996) 259–266.
- [20] F.C. Gouldin, An application of fractals to modeling premixed turbulent flames, *Combust. Flame* 68 (1987) 249–266.
- [21] N.C. Blizard and J.C. Keck, Experimental and theoretical investigation of turbulent burning model for internal combustion engines, *SAE Technical Papers* (1974) 18.
- [22] F. Bozza, G. Fontana, E. Galloni, and E. Torella, 3D-1D analyses of the turbulent flow field, burning speed and knock occurrence in a turbocharged SI engine, *SAE Technical Paper* 2007-24-0029 (2007).
- [23] G.P. Beretta, M. Rashidi, J.C. Keck, Turbulent flame propagation and combustion in spark ignition engines, *Combust. Flame* 52 (1983) 217–245.
- [24] M. Sjerić, D. Kozarac, H. Schuemie, R. Tatschl, A new quasi-dimensional flame tracking combustion model for spark ignition engines, *Energy Convers. Manag.* 165 (2018) 263–275.
- [25] D. Veynante, L. Vervisch, Turbulent combustion modeling, *Prog. Energy Combust. Sci.* 28 (2002) 193–266.
- [26] V.L. Zimont, A.N. Lipatnikov, A numerical model of premixed turbulent combustion of gases, *Chem. Phys. Rep.* 14 (1995) 993–1025.
- [27] V. Karpov, A. Lipatnikov, V. Zimont, A test of an engineering model of premixed turbulent combustion, *Symp. (Int.) Combust.* 26 (1996) 249–257.
- [28] K. Truffin, C. Angelberger, S. Richard, C. Pera, Using large-eddy simulation and multivariate analysis to understand the sources of combustion cyclic variability in a spark-ignition engine, *Combust. Flame* 162 (2015) 4371–4390.
- [29] K. Liu, A.A. Burluka, C.G.W. Sheppard, Turbulent flame and mass burning rate in a spark ignition engine, *Fuel* 107 (2013) 202–208.
- [30] A. Ratzke, T. Schöffler, K. Kuppa, F. Dinkelacker, Validation of turbulent flame speed models for methane-air-mixtures at high pressure gas engine conditions, *Combust. Flame* 162 (2015) 2778–2787.
- [31] M. Reyes, A. Melgar, A. Pérez, B. Giménez, Study of the cycle-to-cycle variations of an internal combustion engine fuelled with natural gas/hydrogen blends from the diagnosis of combustion pressure, *Int. J. Hydrogen Energy* 38 (2013) 15477–15487.
- [32] J.B. Heywood, *Internal Combustion Engines Fundamentals*, McGraw Hill Education, 1988.
- [33] J.C. Dent and N.S. Salama, The measurement of the turbulence characteristics in an internal combustion engine cylinder, *SAE Technical Paper Series* 750886 (1975).
- [34] P.V. Farrell, Examples of in-cylinder velocity measurements for internal combustion engines, *Proc. Inst. Mech. Eng. D: J. Automob. Eng.* 221 (2007) 675–6977.
- [35] F.V.T. Fluixá, B.G. Olavarria, D.I. Hoyos, M. Lawes, Experimental determination of the burning velocity of mixtures of n-heptane and toluene in engine-like conditions, *Flow Turbul. Combust.* 89 (2012) 183–213.
- [36] B. Gimenez, A. Melgar, A. Horrillo Güemes, F. Tinaut, Combustion speed in ICE: thermodynamic model for combustion speed, expansion speed, Mendeley Data Base v1 (2019).
- [37] G. Woschni, A universally applicable equation for the instantaneous heat transfer coefficient in the internal combustion engine, *SAE Technical Paper Series* 670931 (1967).
- [38] C.E. Dumitrescu, V. Padmanaban, J. Liu, An experimental investigation of early flame development in an optical spark ignition engine fueled with natural gas, *J Eng Gas Turbine Power* 140 (2018) 82802.
- [39] H. Schlick, G. Pirker, F. Chmela, A. Wimmer, Weiterentwicklung eines nulldimensionalen brennratenmodells für direktgezündete gasmotoren auf basis der computertomographie (improving the predictive capability of a zero-dimensional combustion model for open-chamber gas-engines based on computer tomography), *Engine Combustion Processes Current Problems and Modern Techniques*, ESYTEC: Erlangen, Munich, Germany (2009), pp. 115–126. IXth Congress.
- [40] A. Wassiljew, Wärmeleitung in gasgemischen, *Phys. Z.* 5 (1904) 737–742 Heft 22, S.
- [41] E.A. Mason, S.C. Saxena, Approximate formula for the thermal conductivity of gas mixtures, *Phys. Fluids* 1 (1958) 361–369.
- [42] R.C. Reid, J.M. Prausnitz, B.E. Poling, *The Properties of Gases & Liquids*, 4th Edition, 1987.
- [43] E.P.J. Linstrom, W.G. Mallard, NIST Chemistry WebBook, NIST Standard Reference Database n 69, National Institute of Standards and Technology, Gaithersburg MD (2018), p. 20899.
- [44] R.G. Abdel-Gayed, K.J. Al-Khishali, D. Bradley, Turbulent burning velocities and flame straining in explosions, *Proc. R. Soc. Lond.* 18 (1984) 517–519.
- [45] N. Fogla, F. Creta, M. Matalon, The turbulent flame speed for low-to-moderate turbulence intensities: hydrodynamic theory vs. experiments, *Combust. Flame* 175 (2017) 155–169.
- [46] V.L. Zimont, Gas premixed combustion at high turbulence. Turbulent flame closure combustion model, *Exp. Thermal Fluid Sci.* 21 (2000) 179–186.
- [47] S.S. Shy, W.J. Lin, K.Z. Peng, High-intensity turbulent premixed combustion: general correlations of turbulent burning velocities in a new cruciform burner, *Proc. Combust. Inst.* 28 (2000) 561–568.
- [48] Y. Kawanabe, H. Shioji, M. Tsunooka, T. Ali, CFD simulation for predicting combustion and pollutant formation in a homogeneous charged SI engine, *Proceedings of the the Fourth International Symposium COMODIA*, 98 (1998), pp. 233–238.
- [49] H. Kido, T. Kitagaw, K. Nakashima, and K. Kato, Improved model of turbulent mass burning velocity, *Memoirs of the Kyushu University, Faculty of Engineering* 49 (1989) 229–247.
- [50] H. Kobayashi, Y. Kawabata, K. Maruta, Experimental study on general correlation of turbulent burning velocity at high pressure, *Symp. (Int.) Combust.* 27 (1998) 941–948.
- [51] J. Wallesten, A.N. Lipatnikov, and J. Nisbet, Turbulent flame speed closure model: further development and implementation for 3-d simulation of combustion in SI engine, *SAE Technical Papers* SAE 982613 (1998) 724.